# Supporting Information for: "Field Effect Optoelectronic Modulation of Quantum-Confined Carriers in Black Phosphorus"

William S. Whitney[1‡], Michelle C. Sherrott[2,3‡], Deep Jariwala[2,3], Wei-Hsiang Lin[2], Hans Bechtel[4], George R. Rossman[5], Harry A. Atwater[2,3*]

1. Department of Physics, California Institute of Technology, Pasadena, CA 91125, USA
2. Thomas J. Watson Laboratory of Applied Physics, California Institute of Technology, Pasadena, CA 91125, USA
3. Resnick Sustainability Institute, California Institute of Technology, Pasadena, CA 91125, USA
4. Lawrence Berkeley National Laboratories, Berkeley, CA 94720, USA
5. Division of Geological and Planetary Sciences, California Institute of Technology, Pasadena, CA 91125, USA

‡ Equal contributors

*Corresponding author: Harry Atwater (haa@caltech.edu)

## I. Extinction Modulation of 25 nm thick Flake

The infrared extinction results are shown in Figure S1 normalized to the zero bias extinction, and show significant modulation of a single broad feature. This feature is strongest at positive bias, and reverses sign twice: it changes polarity as the bias crosses 0 V, and again between -60 V and -120 V.

We interpret our results for the 25 nm sample as an ambipolar Burstein-Moss shift. Because this flake exhibits ambipolar transport, we can understand the primary spectral feature as resulting from three separate regimes of charge carrier modulation. At increasingly positive bias (ie: increased hole doping), Pauli blocking of optical transitions is increased, resulting in higher infrared transmission at lower photon energies. At negative bias, transmission first decreases as we deplete the sample of holes and more optical transitions are allowed, and then increases as the sample becomes electron-doped and a Burstein-Moss effect of the opposite charge carrier type is introduced. This ambipolar, gate-controlled Burstein-Moss shift is the first observed in a two-dimensional semiconductor, to the best of our knowledge. We note the presentation of this data in arbitrary units, as further investigation of modulation strength in thick BP flakes is needed to draw definitive, quantitative conclusions.

Superimposed on this large modulation are small oscillations that are most evident at high applied field – particularly +120 V. We suggest that these oscillations are related to features in the quantized intersubband transitions that occur in the BP optical conductivity, as seen from the calculation in Figure S5d. A further, larger oscillation appears in the -120 V transmittance spectrum near 0.3 eV. We speculate that this feature may result from distinctions between electron and hole-doped optical responses; however further study would be required to draw definitive conclusions about this. We further note that transport measurements for this flake were performed at 80 K, at a pressure of 3mTorr.

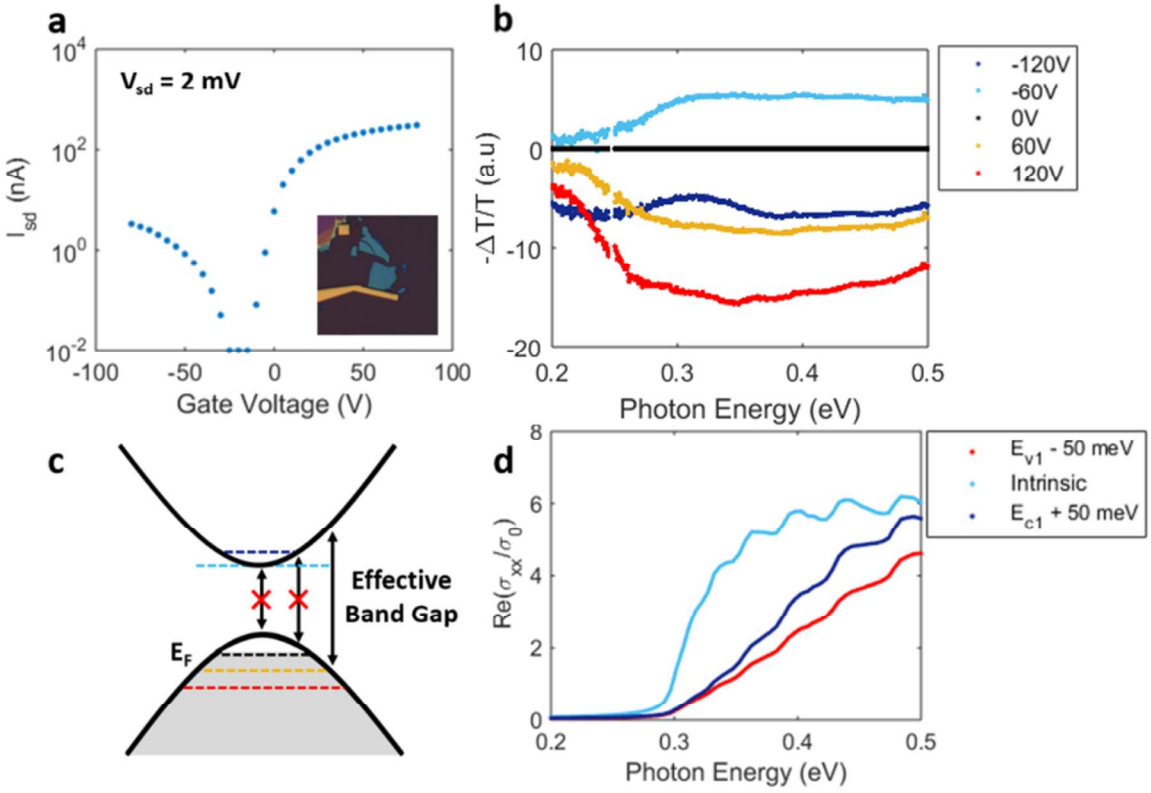


**Figure S1:** Gate modulation of 25 nm flake. **a)** Source-drain current vs gate voltage. Ambipolar conduction is seen. Inset: Optical microscope image of flake. **b)** FTIR e vs photon energy normalized to zero bias. **c)** Schematic of electronic band structure and allowed interband transitions at different voltages. **d)** Calculated optical conductivity of an intrinsic, 10 nm BP quantum well, normalized to the universal conductivity of graphene.

## II. Crystal Lattice Structure

The x (armchair) and y (zig-zag) crystal lattice directions are determined by polarization-dependent visible reflectance measurements. At each angle of polarization an image is recorded, and pixel RGB values are sampled from both the BP flake and nearby substrate. The ratio of green channel values from flake to substrate is averaged over three sample positions, and plotted as a function of polarization angle in Figure S1. Maxima and minima in green reflectance determine the armchair and zig-zag directions, respectively.[1] This characterization was not performed for the samples measured with the internal FTIR glo-bar source, as those measurements are fundamentally unpolarized.

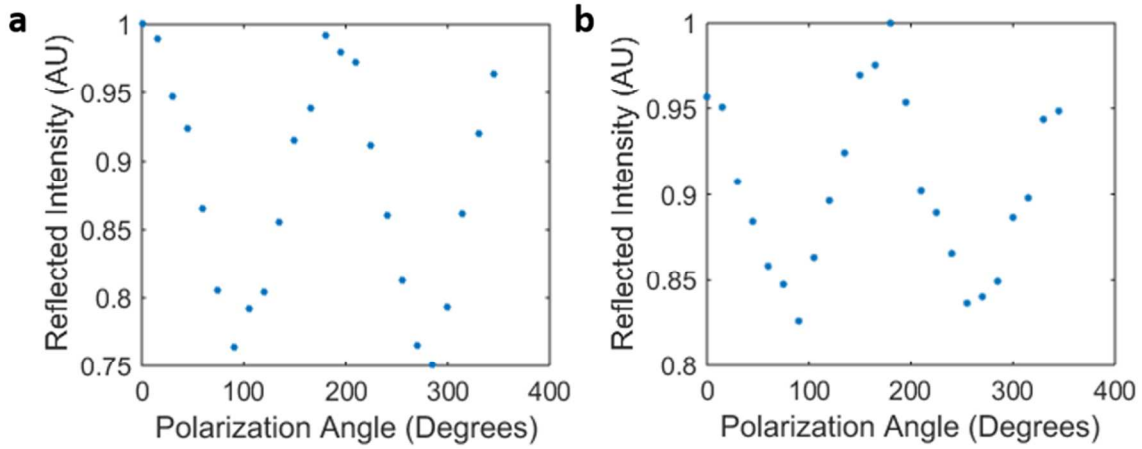


**Figure S2:** Intensity of the green channel of light reflected from BP flakes as the linear polarization of the incident light is rotated for **a)** the 6.5 nm flake and **b)** the 25 nm flake. In both cases, the polarization angle is defined as the angle between the x (armchair) crystal axis and the linear polarizer. The green component of the pixel RGB of the flakes is normalized to that of the adjacent substrate.

## III. Polarization State of Synchrotron FTIR Beam

The FTIR beam used in our final (Fig 4) measurement and Supplement S1 has an inherent elliptical polarization due to its synchrotron source. The polarization state is approximately two to one polarized along the major and minor axes of this ellipse, which are indicated in Figure S3. Due to the complicated polarization state of incident light from the synchrotron, and because a previous study has extensively investigated this

effect experimentally[2], we do not study in detail the anisotropic optical properties of BP. However, since the $\sigma_{xx}$ component of the optical conductivity is one to two orders of magnitude larger than the $\sigma_{yy}$ component, plotted in Figure S4, we argue that the observed optical response derives almost entirely from light-material interactions along the armchair direction. As a result, the only effect of elliptically polarized light is to scale down the observed modulation strength. Probing devices with light of properly aligned polarization – linear along the armchair direction – would maximize this modulation strength; however, the underlying physics would be unchanged.

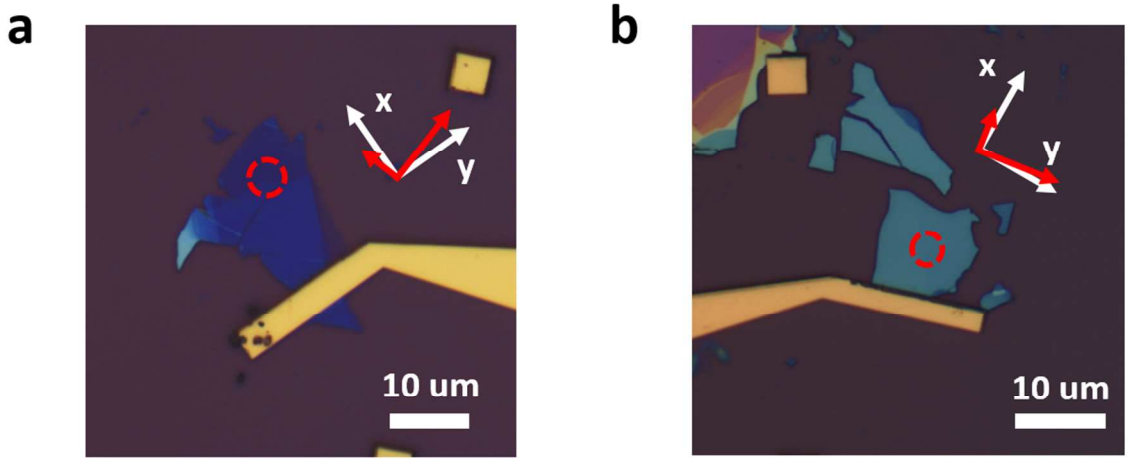


**Figure S3:** Polarization states of FTIR light. The synchrotron infrared source is inherently polarized at ALS beamline 1.4.3, with a roughly 2:1 elliptical polarization in the direction indicated here in red for **a)** the 6.5 nm flake and **b)** the 25 nm flake. Also indicated are the crystal axes, where x and y correspond to the armchair and zig-zag lattice directions, respectively, and the measurement site, indicated by a red, dashed circle.

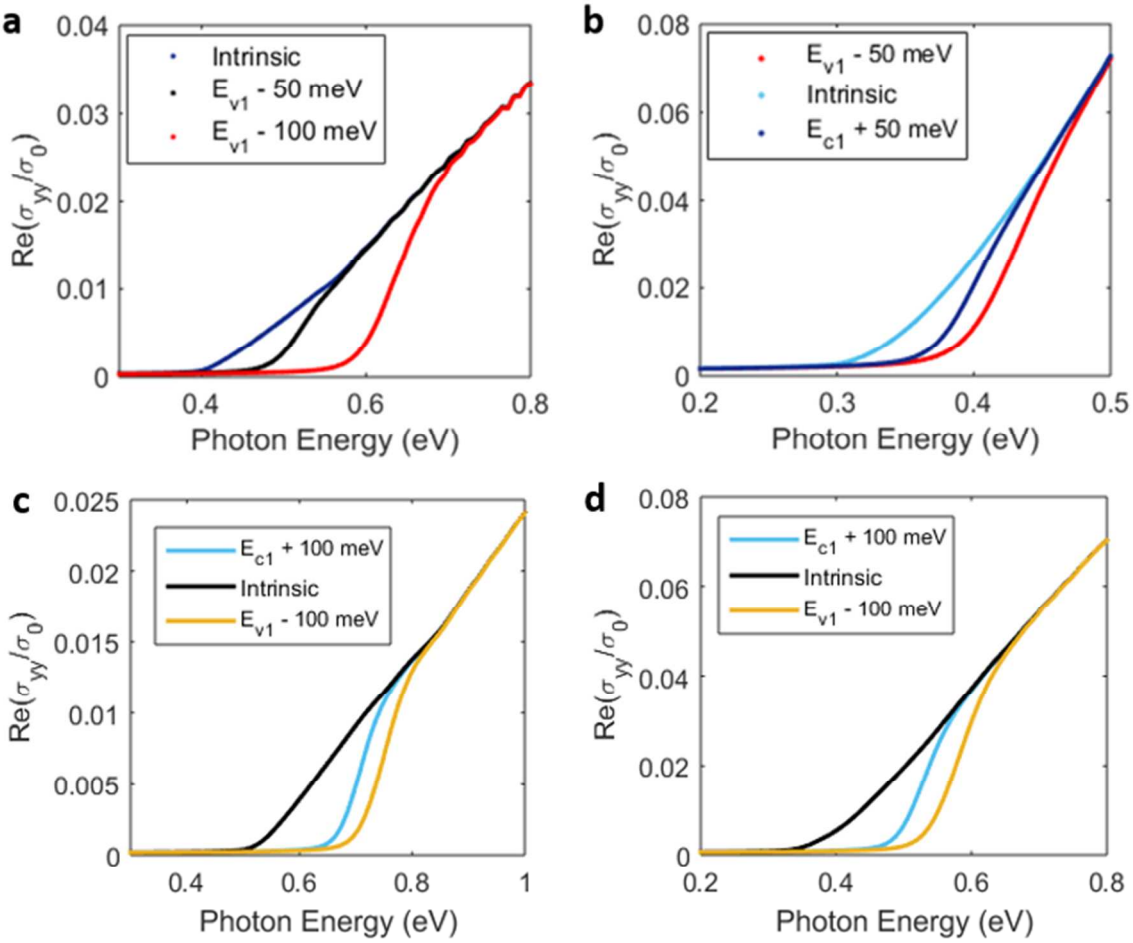


**Figure S4:** Calculated $\sigma_{yy}$ optical conductivities at different Fermi levels for **a)** the 6.5 nm flake, **b)** the 25 nm flake, **c)** the 7 nm flake and **d)** the 14 nm flake. In all cases, $\sigma_{yy}$ is one to two orders of magnitude smaller than $\sigma_{xx}$, implying that the interaction of the FTIR beam with the flake is dominated by the $\sigma_{xx}$. As a result, any polarization of the FTIR beam for measurements of the 6.5 nm and 25 nm flakes effectively scales the gate modulation as the strength of the interaction of the beam with the $\sigma_{xx}$ vs $\sigma_{yy}$ optical conductivity components changes.

## IV. Carrier Concentration Determination

We estimate carrier concentration in our flakes from gated resistance measurements by noting the applied bias at which the flake is approximately charge neutral – ie, least conductive – and using a parallel plate capacitor model to calculate the charge added between that bias and 0 V. For 285 nm silicon oxide, the parallel plate model results in a capacitance per unit area of $c = \varepsilon/d = 12$ nF/cm$^2$. We then calculate $\Delta Q = C\Delta V$.

## V. Accumulation/Depletion Length Determination

We estimate the screening length in our flakes using the Thomas-Fermi method adopted for black phosphorus by Tony Low, et al. The result of this calculation is shown in Figure S5, which describes band bending in the film as a function of depth / thickness. The screening length is of order 3 nm, indicating that band bending yields modulation that varies significantly along the depth axis of our flakes.

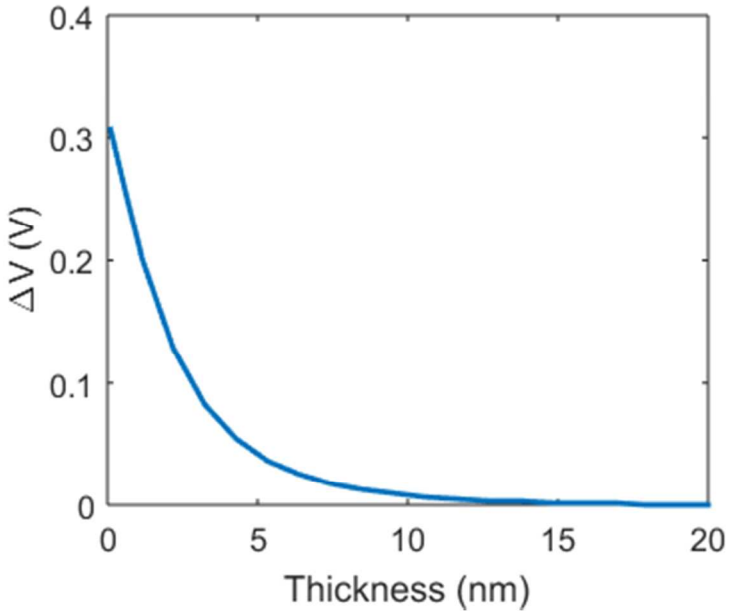


**Figure S5:** Calculated approximate voltage drop across the flake using the Thomas-Fermi method. The screening length is of order 3 nm.

## VI. Thickness Characterization

Atomic Force Microscopy (AFM) was used to determine the nominal thickness of the Black Phosphorus samples analyzed. Scans are shown in Figure S6.

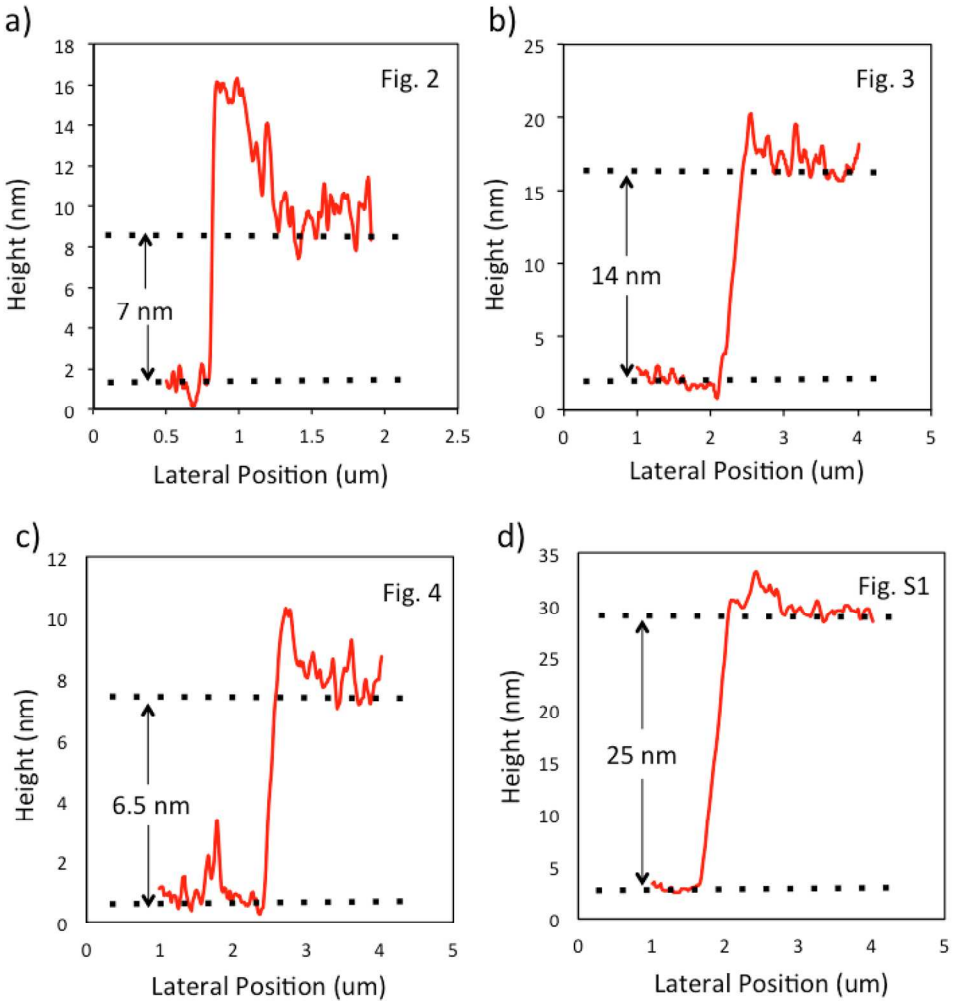


**Figure S6:** AFM Scans of BP samples presented in the main text and Supporting Information. a) Fig. 2, indicating 7 nm thickness b) Fig. 3, indicating 14 nm thickness, c) Fig. 4, indicating 6.5 nm thickness, d) Figure S1, indicating 25 nm thickness.

## VII. Raman Characterization

Raman spectroscopy was used to both compare results to standard literature for black phosphorus, and to characterize oxidation as a function of time. No appreciable change are seen in our encapsulated devices, suggesting that while oxide appears to form at some point during fabrication, it does not continue to form during our measurements.

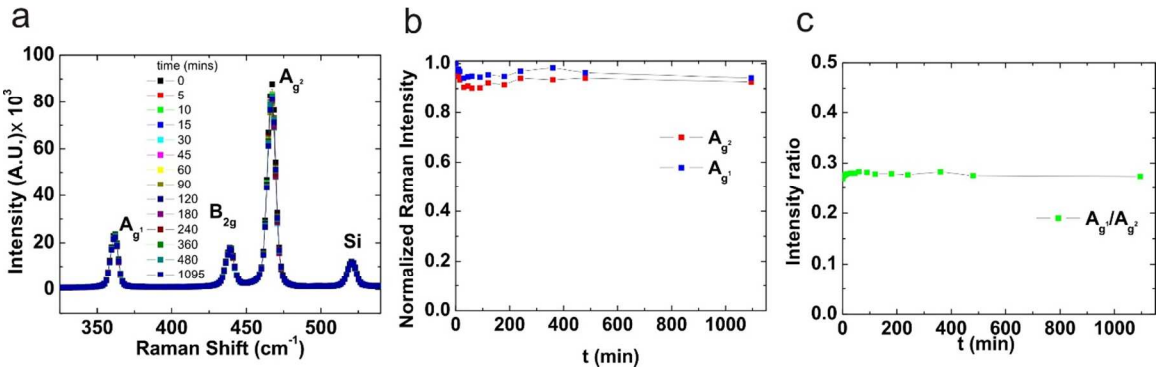


**Figure S7: a)** Raman spectrum of a few layer BP flake using a 514 nm laser showing the $Ag^1$, $B_{2g}$ and $Ag^2$ peaks. The $Ag^2$ peak position suggests a flake thickness of 4-6 nm. Spectra acquired at times ranging from 0 to 1095 mins are overlayed. No appreciable shifts in peak in changes in peak magnitude are visible as a function of time. **b)** Normalized intensity of $Ag^1$ and $Ag^2$ peaks as a function of time again suggesting no signs of oxidation degradation or decay. **c)** Time evolution of ratio of $Ag^1/Ag^2$ (known to be a clear indicator of oxidation) suggesting no appreciable change over 1095 mins further indication of no appreciable oxidation or degradation outside of the initial/immediate oxide formation upon exfoliation.


1. Mao, N.; Tang, J.; Xie, L.; Wu, J.; Han, B.; Lin, J.; Deng, S.; Ji, W.; Xu, H.; Liu, K.; Tong, L.; Zhang, J. *Journal of the American Chemical Society* **2016,** 138, (1), 300-305.
2. Guowei Zhang, A. C., Shenyang Huang, Chaoyu Song, Tony Low,; Yan, H. *arXiv:1607.08049* **2016**.